Received: 16 October 2019 | Revised: 17 February 2021 | Accepted: 1 March 2021

DOI: 10.1111/joa.13429

Journal of Anatomy ANATOMICAL SOCIETY WILEY

ORIGINAL PAPER

Anatomic, computed tomographic, and ultrasonographic assessment of the lymph nodes in presumed healthy adult cats: The head, neck, thorax, and forelimb

Mauricio Tobón Restrepo | **Yvonne Espada** | **Adrià Aguilar** | **Xavier Moll** | **Rosa Novellas**

Departament de Medicina i Cirurgia Animals, Facultat de Veterinària, Universitat Autònoma de Barcelona, Barcelona, Spain

Correspondence
Mauricio Tobón Restrepo, Departament de Medicina i Cirurgia Animals, Facultat de Veterinària, Universitat Autònoma de Barcelona, Barcelona, Spain.
Email: matores79@gmail.com

Funding information
Departamento Administrativo de Ciencia, Tecnología e Innovación

Abstract

Assessment of the lymph nodes is key in staging cancer patients. Descriptions of normal features of the feline lymph nodes using computed tomography (CT) and ultrasound (US) are limited. A prospective anatomic and comparative imaging study was performed. The frequency of identification and the size of the lymph nodes during gross pathology from 6 feline cadavers were compared to the images of lymph nodes from 30 presumed healthy adult cats obtained by CT and US. Measurements (length, width, and height) were compared among techniques. The CT and US features of the identified lymph nodes were also recorded. The frequency of identification of the lymph centers varied among techniques and individually. The mandibular lymph nodes were identified in 100% of the cadavers and in 100% of the healthy cats using CT and US. The medial retropharyngeal lymph nodes were identified in 100% of the cats using CT and US. The deep cervical lymph nodes were not visualized in the cadavers. The cranial mediastinal and tracheobronchial lymph nodes were not visualized using US. Lymph nodes showed a higher length on CT and higher width on US. The height was the most statistically significant variable measurement among techniques. On CT, lymph nodes were most frequently isoattenuating or slightly hypoattenuating to surrounding musculature, with homogeneous contrast enhancement. On US, most lymph nodes were isoechoic or hypoechoic to surrounding fat tissue. The lymph nodes were most frequently elongated or rounded.

KEYWORDS
computed tomography, diagnostic imaging, feline, gross anatomy, lymph node, ultrasound

1 | INTRODUCTION

Lymph node characterization is important in the diagnosis and prognosis of neoplastic and infectious diseases (Nemanic et al., 2015; Nyman, 2005; Nyman & O'Brien, 2007). There is limited information regarding the imaging features of the lymph centers in the cat. Normal values for size, appearance, and ability to depict many of them using computed tomography (CT) and ultrasound (US) are needed.

The Nomina Anatomica Veterinaria (NAV) (NAV, 2017), reports the parotid, mandibular, and retropharyngeal lymph centers in the head, the superficial and deep cervical lymph centers in the neck, and the axillary lymph center in the forelimb. The lymph centers in the thorax are divided into parietal and visceral. The parietal division includes those located on the inner side of the thoracic wall: the dorsal and ventral thoracic lymph centers. The visceral division includes those located in the mediastinal

region: the mediastinal and bronchial lymph centers (NAV, 2017; Tompkins, 1993).

The length of the lymph nodes in the cat has been reported in the anatomy literature mainly based on the studies made in Japan in the 1950s; however, width and height were not reported (Saar & Getty, 1982; Sugimura et al., 1955).

A study describing the normal features of the feline medial retropharyngeal lymph node using noncontrast CT and US has been published (Nemanic & Nelson, 2012). A mild (CT) or moderate (US) heterogeneous parenchyma was considered normal for this lymph node. However, contrast medium was not used on CT (Nemanic & Nelson, 2012). More recently, the CT appearance of some intrathoracic lymph nodes has been published (Smith et al., 2019). However, descriptions of the normal CT and US features and comparisons between techniques of the feline parotid, mandibular, superficial and deep cervical, axillary, mediastinal, and ventral thoracic lymph centers are currently not available.

The aims of this study were (i) to compare the frequency of identification and dimensions of lymph nodes from the lymph centers of the head, neck, thorax, and forelimb obtained with CT and US in a group of healthy adult cats to the measurements obtained from an anatomic study and (ii) to describe the CT and US features of these lymph nodes in healthy adult cats.

2 | MATERIALS AND METHODS

This prospective anatomic and comparative imaging study was approved by the ethical committee of the Universitat Autònoma de Barcelona with the reference number CEAAH 2255 of September 2013. Owner consent for all the patients and cadavers included in the study was also obtained.

2.1 | Lymph centers

The lymph centers that were studied are the parotid (comprising the superficial parotid lymph node), mandibular (comprising the medial and lateral mandibular lymph nodes), retropharyngeal (comprising the medial and lateral retropharyngeal lymph nodes), superficial cervical (comprising the dorsal and ventral superficial cervical lymph nodes), deep cervical (comprising the middle and caudal deep cervical lymph nodes), axillary (comprising the axillary and accessory axillary lymph nodes); dorsal thoracic (comprising the thoracic aortic and intercostal lymph nodes), ventral thoracic (comprising the sternal, phrenic, and superficial cranial epigastric lymph nodes), mediastinal (comprising the cranial mediastinal lymph nodes), and bronchial (comprising the left, right, and middle tracheobronchial, and pulmonary lymph nodes).

2.2 | Anatomical study

Feline cadavers referred for necropsy to the pathology department were prospectively included from January 2013 to June 2015. Inclusion criteria were time of death within 24 h, being older than 1 year of age, and cause of death unrelated to inflammatory or neoplastic processes according to the clinical history and pathology report.

All the dissections were performed by the first author (M.T.R). Lymph nodes of the head, neck, thorax, and forelimb were searched following previous anatomic descriptions (Saar & Getty, 1982; Tompkins, 1993). Postmortem coloring procedures for the lymphatic system were not performed.

The frequency of lymph node identification per lymph center and anatomical landmarks were recorded. The length, width, and height of each lymph node were measured using a manual dial caliper (Vernier 0–150 mm/0.02 high precision). The length was defined as the largest dimension in the rostro/craniocaudal plane. The width was measured at the thickest point in the mediolateral plane. The height was measured at the thickest point in the dorsoventral plane.

2.3 | Imaging study

Healthy cats older than 1 year of age were recruited at the Fundació Hospital Clinic Veterinari of the Universitat Autònoma de Barcelona from staff, students, and hospital clients from October 2013 to July 2015. Cat's health status was based on a physical examination performed randomly by two of the authors (A.A and X.M), biochemical profile (including calcium, glucose, potassium, total proteins, alanine-amino-transferase, gamma-glutamyl-transferase, cholesterol, urea, and creatinine), and complete blood count. A fast test to rule out the presence of feline immunodeficiency virus antibodies and feline leukemia virus antigens (SNAP® combo plus, IDEXX, USA) and a polymerase chain reaction test to rule out the presence of *Bartonella* sp were also performed. All the CT and US images were acquired and reviewed by the first author (M.T.R), under the supervision of a board-certified veterinary radiologist (R.N) and a radiology professor (Y.E).

2.4 | Computed tomography

The animals were sedated with intramuscular midazolam (Midazolam 15 mg/3 ml, Normon, Spain) at a dose of 0.2 mg/kg, butorphanol (Torbugesic® 10 mg/ml, Zoetis, Spain) at a dose of 0.4 mg/kg and ketamine (Imalgene® 100 mg/ml, Merial, Spain) at a dose of 5 mg/kg. The cats were intubated, and inhalation anesthesia was maintained with Isoflurane 1.5%–2% (Isoflurane, Abbott Laboratories, UK) in 100% of O_2, using a Mapleson F circuit and a fresh gas flow of 600 ml/kg min. The patients were positioned on the CT table in dorsal recumbency with the limbs extended at the sides. A whole body scan was performed before and after manual intravenous administration of Iopromide (Ultravist 300 mg/ml, Bayer pharma AG, Germany) or Iopamidol (Scanlux 300 mg/ml, Sanochemia pharmazeutika, Austria) in the cephalic vein at a dose of 2 ml/kg.

Scans were performed with a 16-slice helical CT-scanner (GE Brivo CT 385, Madrid, Spain) with a slice thickness of 0.625 mm, interval thickness of 0.625 mm, collimation pitch of 0.5625:1, 120 kV, 50–90 mA, field-of-view according to patient size, and a matrix of 512 × 512. All data were reformatted in transverse plane and soft tissue algorithm and recorded for further analysis using an image archiving and communication system software (Centricity PACS-IW, GE healthcare, Spain).

2.5 | Image analysis

The frequency of lymph node identification per lymph center using precontrast and postcontrast CT images were recorded. Length was determined using two previously reported methods (Beukers et al., 2013; Nemanic & Nelson, 2012): (i) CT-Calculated length: multiplying the slice thickness by the number of transverse images that contained the lymph node and (ii) CT-Measured length: after generating a sagittal image of the lymph node's maximal dimension with multiplanar reconstruction, an electronic caliper was placed from the rostral/cranial to the caudal border to measure the length. Width and height were measured in transverse images at the rostral/cranial, middle, and caudal aspects of each lymph node following the same directions as described for the anatomic study. The highest values of height and width per lymph node were used for statistical analysis. A short-to-long axis ratio was calculated dividing the higher value of height by the value of CT-Measured length. The shape of the lymph nodes was classified as rounded, elongated, or miscellaneous as previously reported (Beukers et al., 2013; Nyman, 2005). A lymph node was defined as rounded when the short-to-long axis ratio was ≥0.5. A short-to-long axis ratio <0.5 was used to classify a lymph node as elongated. Lymph nodes with a multilobular structure that did not fit the ratio were classified as miscellaneous. Precontrast and postcontrast attenuation (Hounsfield units) values were determined by placing a circular/oval region of interest (ROI) of 2–4 mm^2 over the same rostral/cranial, middle, and caudal transverse slice where width and height measurements were performed (Figure 1a,b). In small lymph nodes, ROIs were made as large as possible inside the lymph node margins. Average of precontrast and postcontrast attenuation values per lymph node were calculated using the three obtained measurements. As in previously reported studies (Nemanic & Nelson, 2012), lymph nodes attenuation was compared with the surrounding muscles and was classified as isoattenuating, slightly hypoattenuating (slightly less attenuating and homogeneous), hypoattenuating (markedly less attenuating and homogeneous), hyperattenuating, and heterogeneous (single or multiple areas of different attenuation within the lymph node). Following the administration of contrast medium, the attenuation was classified as homogeneous, mildly heterogeneous (small, multiple areas of different contrast enhancement), heterogeneous (large, multiple areas of different contrast enhancement), and peripheral enhancement (contrast enhancement in a ring-like distribution with a hypoattenuating center).

2.6 | Ultrasound

Ultrasound was performed immediately after the CT-scan with maintained inhalational anesthesia. The hair of the ventral aspect of the neck, cranial aspect of the scapulae, and the region of the sternum was clipped. The animals were positioned in dorsal recumbency with the neck extended. Right and left lateral recumbency were also used when the superficial cervical lymph nodes were assessed. US examinations were performed using an ultrasound machine (Esaote Mylab70 Xvision®, Firenze, Italy) with a 4–13 MHz frequency linear transducer. Technical settings were adjusted to obtain the optimal images of the lymph nodes in all the animals. Acoustic coupling gel (Transonic gel®, Telic, Barcelona, Spain) was applied to ensure adequate skin-transducer contact. Sagittal and transverse images of each lymph node were recorded.

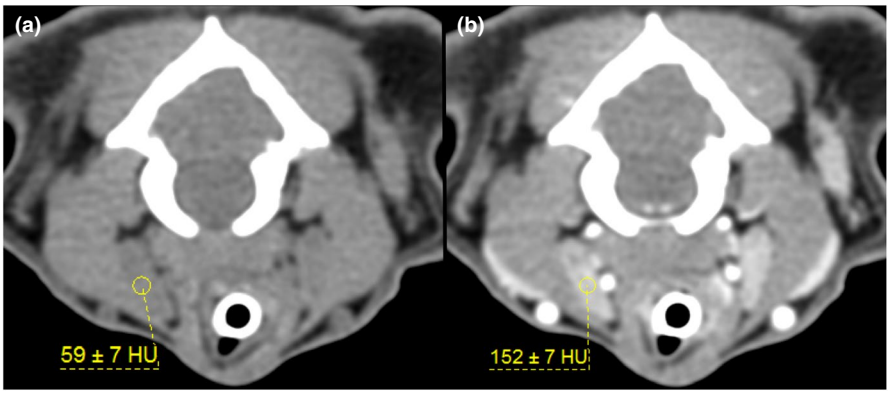

FIGURE 1 Representation of a region of interest (ROI) for the measurements of the Hounsfield units. (a) Transverse precontrast computed tomography (CT) slice of the medial retropharyngeal lymph node. (b) Transverse postcontrast CT slice of the same lymph node and same cat. A circular ROI (yellow circle) is placed in the center of the lymph node. The average and standard deviation of the Hounsfield units within the ROI are displayed

2.7 | Image analysis

The frequency of lymph node identification per lymph center was recorded. A sagittal image of the lymph node that included its longest dimension was obtained by placing the transducer with the guide pointing rostral/cranial, parallel (or slightly oblique) to the spine. In this image, the length was measured using an electronic caliper from the rostral/cranial to the caudal border. The height was measured in the same image perpendicularly to the length at the point of maximum thickness (dorsal to ventral). The width was measured in a transverse image of the lymph node. The transducer was rotated 90° with the guide towards the right side of the patient, and an image that contained the widest portion of the lymph node was recorded. The short-to-long axis ratio was calculated by dividing height by length and used to determine the shape of the lymph node following the same criteria as on CT.

Lymph node echogenicity was recorded as homogeneously hypoechoic, isoechoic, hyperechoic, or heterogeneous when compared to surrounding fat. The presence of a hyperechoic central line that corresponds with the hilus was also recorded. Margins were defined as smooth or irregular.

2.8 | Statistics

Sample determination was calculated based on the population of the feline patients presented at the Fundació Hospital Clinic Veterinari of the Universitat Autònoma de Barcelona. A confidence interval of 95% and an error margin of 5%–1% was set. Thirty cats were determined to be adequate to reach statistical power. Data were digitalized using Excel (Microsoft office Excel, 2010, USA). Statistic tests were selected by the first author (M.T.R) and a statistician. Statistical analysis was performed using the free available statistics software R (R 3.2.3, 2015-12-10). Continous variables were presented as mean (standard deviation) and categorical variables as number (percentage). Nonparametric tests were used to compare the median (values not reported) of the categorical variables. Wilcoxon Signed Rank Test was used to compare the pair distribution between the CT-Calculated and CT-Measured lengths of the lymph nodes. After this, the CT-Measured length was used in the pair comparison with the US. The width and height of lymph nodes in CT versus US were also compared with Wilcoxon Signed Rank Test. Mann–Whitney *U* test was used to compare the pair distribution of the lymph node measurements (CT-Measured length, width, and height) between CT and anatomy and between US and anatomy. Each measurement was compared individually for each lymph center and not for the total number of identified lymph nodes per cat (no post hoc corrections were used). $p < 0.05$ was considered statistically significant.

3 | RESULTS

Six feline cadavers were included in the anatomic study. Causes of death determined by necropsy were heart failure ($n = 2$), kidney failure ($n = 2$), poisoning ($n = 1$), and trauma ($n = 1$). The average age was 6.8 years (range 1–16). Five cats were domestic shorthairs, and one cat was a British longhair. This group included two entire females, two neutered females, and two neutered males.

Following exclusion of four cats because of positive results for *Bartonella* sp ($n = 3$) and feline immunodeficiency virus antibodies and feline leukemia virus antigens ($n = 1$), a total of 30 cats with an unremarkable biochemical, serological, complete blood test, and physical examination were included in the imaging study. Mean age and weight were 3.7 years (range 1.5–17) and 4.4 kg (range 3.0–7.0), respectively. Twenty-nine cats were domestic shorthairs, and one cat was a Persian. The group included 5 entire males, 6 neutered males, 9 entire females, and 10 neutered females.

Computed tomography showed a higher frequency of lymph nodes identification when compared to US and anatomy (Table 1).

Lymph node measurements per technique are summarized in Table 2. The comparison of the CT-Calculated length versus the CT-Measured length showed statistically significant differences. Therefore, the CT-Measured length was chosen for further comparison with US and anatomic lengths because it was considered to produce a more reliable dimension of the lymph nodes. In overall, lymph nodes were longer and thicker on CT than on US and anatomy. The largest differences were found in the medial retropharyngeal lymph nodes which were ±7.0 mm longer than in US and anatomy. The lymph nodes were relatively wider in US than on CT and anatomy.

Most lymph nodes were isoattenuating or slightly hypoattenuating to the surrounding musculature and showed homogeneous contrast enhancement (Table 3). Only the sternal (71.4%) and the axillary (R: 27.6%; L: 25%) lymph nodes presented heterogeneous attenuation in precontrast and postcontrast images.

Most lymph nodes were elongated or rounded (Table 4). Nevertheless, the medial retropharyngeal, dorsal superficial cervical, and accessory axillary lymph nodes occasionally presented a miscellaneous shape. Most lymph nodes were isoechoic or hypoechoic to surrounding fat (Table 5). The axillary lymph nodes showed a high frequency of heterogeneous echogenicity compared with the rest of the lymph nodes. The lymph node hilus was rarely identified and only seen in the mandibular (2.5%), medial retropharyngeal (9.5%), superficial cervical (6.8%), axillary (13.5%), and sternal (10.0%) lymph nodes.

3.1 | Lymph center description: Parotid lymph center (lymphocentrum parotideum)

The parotid lymph nodes were identified slightly rostral or in contact with the parotid salivary gland (Figure 2a–d). The duct of this gland ran ventrally to the lymph node, and the temporal superficial vessels ran dorsally. Fat tissue was found around the lymph node. On CT images, the close contact of the parotid lymph node with the parotid salivary gland compromised their differentiation from the glandular tissue. However, the administration of contrast medium improved the visualization of these lymph nodes in some animals. In 1/30 cats,

TABLE 1 Frequency of identification of the lymph nodes in each technique

Lymph center	Lymph node	CT, n (%)	US, n (%)	Anatomy, n (%)
Parotid	RP	9 (30.00)	0 (0.00)	3 (50.00)
	LP	12 (40.00)	1 (3.33)	3 (50.00)
Mandibular	RMMn	30 (100.00)	30 (100.00)	6 (100.00)
	RLMn	30 (100.00)	30 (100.00)	6 (100.00)
	LMMn	30 (100.00)	30 (100.00)	6 (100.00)
	LLMn	30 (100.00)	30 (100.00)	6 (100.00)
Retropharyngeal	RMR	30 (100.00)	30 (100.00)	3 (50.00)
	LMR	30 (100.00)	30 (100.00)	5 (83.33)
Superficial cervical	RDSC1	25 (83.33)	29 (96.67)	0 (0.00)
	RDSC2	30 (100.00)	9 (30.00)	4 (66.67)
	RVSC	29 (96.67)	2 (6.67)	4 (66.67)
	LDSC1	24 (80.00)	25 (83.33)	0 (0.00)
	LDSC2	29 (96.67)	6 (20.00)	6 (100.00)
	LVSC	25 (83.33)	2 (6.67)	4 (66.67)
Deep cervical	CDC	11 (36.67)	0 (0.00)	0 (0.00)
Axillary	RAx	29 (96.67)	30 (100.00)	4 (66.67)
	LAx	28 (93.33)	29 (96.67)	3 (50.00)
	RAAx1	30 (100.00)	5 (16.67)	1 (16.67)
	RAAx2	9 (30.00)	1 (3.33)	0 (0.00)
	LAAx1	30 (100.00)	3 (10.00)	1 (16.67)
	LAAx2	8 (26.67)	0 (0.00)	0 (0.00)
	LAAx3	1 (3.33)	0 (0.00)	0 (0.00)
Ventral thoracic	S	22 (73.33)	17 (56.67)	4 (66.67)
Mediastinal	CrM	16 (53.33)	0 (0.00)	5 (83.33)
Bronchial	MTB	24 (80.00)	0 (0.00)	6 (100.00)
	RTB	6 (20.00)	0 (0.00)	6 (100.00)
	LTB	12 (40.00)	0 (0.00)	6 (100.00)

Abbreviations: CDC, caudal deep cervical; CrM, cranial mediastinal; CT, computed tomography; LAAx1, LAAx2, and LAAx3, left accessory axillary; LAx, left axillary; LDSC1 and LDSC2, left dorsal superficial cervical; LLMn, left lateral mandibular; LMMn, left medial mandibular; LMR, left medial retropharyngeal; LP, left parotid; LTB, left tracheobronchial; LVSC, left ventral superficial cervical; MTB, medial tracheobronchial; RAAx1 and RAAx2, right accessory axillary; RAx, right axillary; RDSC1 and RDSC2, right dorsal superficial cervical; RLMn, right lateral mandibular; RMMn, right medial; RMR, right medial retropharyngeal mandibular; RP, right parotid; RTB, right tracheobronchial; RVSC, right ventral superficial cervical; S, sternal; US, ultrasound.

only one parotid lymph node was identified on US images, rostral to the left parotid salivary gland.

3.2 | Mandibular lymph center (lymphocentrum mandibulare)

In the cadavers, two mandibular lymph nodes were identified on each side of the mandibular angle, cranial to the mandibular salivary gland. They correspond to the right lateral, right medial, left lateral, and left medial mandibular lymph nodes. As an anatomic landmark, the linguofacial vein ran between these lymph nodes (Figure 3a). On CT and US, these four mandibular lymph nodes were identified in all the cats. On CT images, they were most frequently isoattenuating to the surrounding muscles, which hindered their identification in thin cats. However, simultaneous assessment of precontrast and postcontrast images helped the localization of these lymph nodes on the precontrast images (Figure 3c,d). On US, the linguofacial vein was identified with color Doppler and helped to localize the medial and lateral mandibular lymph nodes (Figure 3b).

3.3 | Retropharyngeal lymph center (lymphocentrum retropharyngeum)

It consists of the medial and the lateral retropharyngeal lymph nodes. In the present anatomic and imaging study, only the medial could be identified. In the anatomic study, the medial retropharyngeal lymph nodes were commonly identified medial to the mandibular salivary gland and the *M. sternocephalicus*, ventral to the caudal

TABLE 2 Mean and standard deviation for length, width, and height of the lymph nodes of the head, neck, forelimb, and thorax

	Length (mm)							
Lymph node	CT-Meas., m (SD)	CT-Calc., m (SD)	US, m (SD)	Anatomy, m (SD)	Meas. versus Calc.[a]	CT-Meas. versus US [a]	CT-Meas. versus Anatomy[b]	US versus Anatomy[b]
RP	5.56 (1.26)	6.57 (1.85)	–	5.00 (0.85)				
LP	5.62 (2.05)	6.37 (2.17)	10.00 (NC)	4.90 (0.26)				
RMMn	11.04 (3.03)	11.41 (3.47)	9.83 (2.84)	8.28 (4.82)	*	**		
RLMn	10.86 (3.23)	11.63 (3.92)	9.71 (2.28)	9.87 (2.24)		*		
LMMn	11.35 (2.77)	11.42 (3.65)	9.01 (2.67)	10.33 (3.28)		**	**	
LLMn	11.32 (2.45)	11.38 (3.35)	9.87 (2.08)	9.67 (2.75)		**	**	
RMR	21.25 (4.27)	18.63 (6.19)	13.38 (3.84)	7.63 (4.65)	**	**	**	*
LMR	20.42 (3.38)	17.77 (5.85)	14.26 (3.82)	13.90 (4.95)	**	**	*	
RDSC[1]	8.18 (3.65)	8.35 (3.57)	7.37 (4.39)	–				
RDSC[2]	6.73 (3.19)	8.30 (4.22)	8.38 (3.60)	9.35 (4.11)				
RVSC	7.92 (2.21)	8.18 (2.70)	10.15 (1.20)	11.25 (2.88)			*	
LDSC[1]	8.44 (4.02)	8.04 (3.98)	6.34 (2.39)	–				
LDSC[2]	6.03 (3.00)	7.54 (3.15)	7.48 (3.55)	7.55 (3.18)	**			
LVSC	8.28 (2.07)	8.72 (2.40)	9.70 (1.27)	12.07 (1.54)			**	
CDC	7.49 (3.81)	8.13 (3.64)	–	–				
RAx	8.82 (1.98)	9.62 (4.01)	7.80 (1.96)	8.28 (3.80)		**		
LAx	9.24 (2.01)	9.73 (2.47)	7.23 (1.73)	8.80 (2.79)		**		
RAAx[1]	14.18 (4.65)	14.48 (4.62)	9.30 (5.63)	17.00 (NC)				
RAAx[2]	6.69 (2.47)	7.80 (3.92)	6.30 (NC)	–				
LAAx[1]	13.43 (6.07)	13.71 (5.57)	9.77 (2.65)	5.9 (NC)	**			
LAAx[2]	9.54 (5.28)	9.80 (5.14)	–	–				
LAAx[3]	4.60 (NC)	5.00 (NC)	–	–				
S	12.24 (3.25)	13.59 (5.43)	7.35 (2.42)	8.62 (3.83)		**		
CrM	8.14 (4.03)	8.02 (4.09)	–	5.66 (2.44)				
MTB	4.82 (1.26)	5.59 (1.88)	–	6.32 (3.07)	*			
RTB	4.03 (0.77)	4.40 (1.13)	–	5.20 (2.41)	*			
LTB	5.62 (2.12)	5.86 (2.43)	–	6.45 (3.15)				

	Width (mm)						Height (mm)					
Lymph node	CT, m (SD)	US, m (SD)	Anatomy, m (SD)	CT, versus US[a]	CT versus Anatomy[b]	US versus Anatomy[b]	CT, m (SD)	US, m (SD)	Anatomy, m (SD)	CT versus US[a]	CT versus Anatomy[b]	US versus Anatomy[(B)]
RP	3.52 (0.63)	–	3.17 (1.36)				4.43 (1.24)	–	1.43 (0.51)		*	
LP	3.19 (0.68)	9.30 (NC)	2.23 (0.55)				4.74 (1.15)	3.80 (NC)	1.30 (0.61)		*	

(Continues)

TABLE 2 (Continued)

Lymph node	Width (mm)						Height (mm)					
	CT, m (SD)	US, m (SD)	Anatomy, m (SD)	CT, versus US[a]	CT versus Anatomy[b]	US versus Anatomy[b]	CT, m (SD)	US, m (SD)	Anatomy, m (SD)	CT versus US[a]	CT versus Anatomy[b]	US versus Anatomy[(B)]
RMMn	5.71 (1.78)	6.83 (2.07)	4.38 (1.46)	**		**	2.87 (1.13)	2.66 (0.95)	1.60 (0.30)		**	**
RLMn	6.53 (1.65)	7.85 (1.95)	4.63 (0.82)	**	**	**	3.22 (0.95)	2.84 (0.81)	1.72 (0.41)	*	**	**
LMMn	5.40 (1.67)	6.23 (1.53)	4.42 (1.26)	**	**		2.84 (0.99)	2.51 (0.55)	1.70 (0.24)	*	**	
LLMn	6.88 (1.82)	7.60 (1.93)	4.23 (0.90)	**	**		3.43 (0.98)	3.05 (0.76)	1.52 (0.38)	**	**	
RMR	6.10 (8.54)	13.33 (3.22)	4.67 (3.76)	**		*	11.92 (2.41)	4.49 (1.14)	1.80 (0.82)	**	**	**
LMR	4.79 (2.03)	11.62 (2.46)	7.38 (2.73)	**	*	**	11.95 (2.47)	4.40 (1.37)	3.94 (3.16)	**	**	
RDSC[1]	4.56 (1.94)	8.21 (3.12)	–	**			4.85 (2.96)	2.51 (0.70)	–	**		
RDSC[2]	4.55 (1.05)	10.38 (5.21)	2.75 (2.09)	**		**	11.53 (4.80)	2.88 (0.79)	1.32 (0.85)	**	**	*
RVSC	3.72 (0.83)	6.60 (2.12)	3.12 (1.00)				4.00 (1.96)	3.40 (0.57)	1.20 (0.44)		**	
LDSC[1]	4.73 (1.96)	7.50 (3.97)	–	**			5.40 (2.26)	2.34 (0.66)	–	**		
LDSC[2]	4.36 (1.06)	7.98 (4.47)	2.85 (1.70)	*		**	10.36 (4.24)	2.40 (0.64)	1.25 (0.76)	*	**	*
LVSC	3.86 (1.21)	8.60 (3.11)	3.6 (1.79)				4.04 (1.70)	4.60 (0.28)	1.45 (0.98)		**	
CDC	3.19 (1.11)	–	–				3.38 (2.43)	–	–			
RAx	3.18 (1.02)	4.93 (1.08)	3.25 (1.21)	**		*	4.03 (1.48)	3.30 (0.97)	1.20 (0.36)	*	**	**
LAx	3.91 (1.45)	4.73 (1.20)	2.40 (0.66)	*		**	4.51 (1.65)	3.52 (1.12)	1.20 (0.17)	*	**	**
RAAx[1]	3.03 (1.04)	5.88 (2.14)	1.40 (NC)				4.38 (1.98)	2.48 (1.31)	0.70 (NC)			
RAAx[2]	2.81 (1.28)	6.50 (NC)	–				3.50 (1.24)	1.30 (NC)	–			
LAAx[1]	3.09 (1.13)	6.50 (1.59)	3.20 (NC)				3.98 (1.73)	2.87 (0.85)	2.00 (NC)			
LAAx[2]	2.85 (1.00)	–	–				3.65 (0.59)	–	–			
LAAx[3]	2.70 (NC)	–	–				4.10 (NC)	–	–			
S	3.88 (1.27)	4.96 (1.21)	4.28 (2.13)				5.20 (1.46)	3.72 (1.18)	2.25 (0.42)	*	**	*
CrM	3.26 (1.24)	–	3.84 (2.13)				3.42 (1.67)	–	1.88 (1.25)		*	
MTB	3.23 (0.99)	–	2.55 (1.13)				2.42 (0.59)	–	1.23 (0.50)		**	
RTB	3.87 (1.19)	–	2.03 (0.61)		**		3.25 (0.57)	–	1.20 (0.51)		**	
LTB	3.19 (1.12)	–	2.60 (1.26)				3.01 (1.00)	–	1.15 (0.33)		**	

Comparison among techniques.

Abbreviations: CDC, caudal deep cervical; CrM, cranial mediastinal; CT-Calc., CT-calculated; CT-Meas., CT-Measured; LAAx1, LAAx2, and LAAx3, left accessory axillary; LAx, left axillary; LDSC1 and LDSC2, left dorsal superficial cervical; LLMn, left lateral mandibular; LMMn, left medial mandibular; LMR, left medial retropharyngeal; LP, left parotid; LTB, left tracheobronchial; LVSC, left ventral superficial cervical; MTB, medial tracheobronchial; NC, not calculated; RAAx1 and RAAx2, right accessory axillary; RAx, right axillary; RDSC1 and RDSC2, right dorsal superficial cervical; RLMn, right lateral mandibular; RMMn, right medial mandibular; RMR, right medial retropharyngeal; RP, right parotid; RTB, right tracheobronchial; RVSC, right ventral superficial cervical; S, sternal; SD, standard deviation; US, ultrasound.

[a]Wilcoxon signed rank test.

[b]Mann–Whitney *U* test.

*$p < 0.05$.

**$p < 0.01$.

TABLE 3 Computed tomographic characteristics of the lymph nodes of the head, neck, forelimb, and thorax of healthy cats

	HU precontrast				HU postcontrast				Attenuation precontrast (%)					Attenuation postcontrast (%)			
Lymph node	Mean	SD	Min	Max	Mean	SD	Min	Max	Iso	S Hypo	Hypo	Hyper	Heter	Hom	S Het	Het	Peri
RP	36.52	9.53	18.67	50.67	131.67	55.46	65.00	257.67	88.89	11.11	0.00	0.00	0.00	100.00	0.00	0.00	0.00
LP	33.94	7.16	20.33	44.00	100.03	30.99	45.33	154.33	83.33	16.67	0.00	0.00	0.00	83.33	0.00	16.67	0.00
RMMn	38.74	11.98	12.33	60.67	137.07	33.46	60.00	209.67	63.33	20.00	16.67	0.00	0.00	90.00	6.67	3.33	0.00
RLMn	36.38	12.48	12.67	63.33	130.84	34.81	52.00	203.67	63.33	20.00	16.67	0.00	0.00	86.67	10.00	3.33	0.00
LMMn	38.54	14.52	6.00	57.67	134.43	33.64	68.33	195.67	63.33	20.00	16.67	0.00	0.00	86.67	6.67	6.67	0.00
LLMn	37.08	10.86	12.00	54.33	130.15	31.64	65.67	182.67	60.00	23.33	16.67	0.00	0.00	80.00	13.33	6.67	0.00
RMR	44.50	6.63	25.67	61.67	133.14	25.42	88.33	183.00	26.67	60.00	13.33	0.00	0.00	40.00	53.33	6.67	0.00
LMR	43.32	7.46	24.67	55.67	131.99	27.61	90.00	184.33	26.67	60.00	13.33	0.00	0.00	37.93	55.17	6.90	0.00
RDSC[1]	22.77	20.46	−39.67	50.00	92.71	30.12	30.33	159.67	52.00	28.00	8.00	0.00	12.00	88.00	0.00	0.00	12.00
RDSC[2]	31.71	15.52	−11.67	60.67	115.79	20.31	71.67	154.67	56.67	36.67	3.33	0.00	3.33	90.00	3.33	6.67	0.00
RVSC	32.76	13.84	1.00	59.00	122.14	28.99	60.00	177.67	44.83	37.93	10.34	0.00	6.90	79.31	10.34	6.90	3.45
LDSC[1]	25.67	23.48	−25.33	62.33	95.01	35.81	5.33	161.67	54.17	29.17	4.17	0.00	12.50	87.50	0.00	0.00	12.50
LDSC[2]	31.90	14.06	−9.00	58.33	116.09	24.08	67.00	154.67	64.29	32.14	3.57	0.00	0.00	96.43	0.00	3.57	0.00
LVSC	35.09	15.25	−19.67	51.33	119.36	31.78	52.00	176.00	56.00	28.00	4.00	0.00	12.00	80.00	8.00	8.00	4.00
CDC	33.03	19.80	−13.33	54.00	94.64	23.99	42.67	128.33	72.73	9.09	0.00	0.00	18.18	63.64	18.18	9.09	9.09
RAx	15.14	20.37	−29.67	54.33	77.62	36.51	17.33	147.67	17.24	48.28	3.45	3.45	27.59	41.38	17.24	0.00	41.38
LAx	20.08	19.43	−19.33	53.67	80.88	33.38	32.00	137.00	17.86	50.00	3.57	3.57	25.00	46.43	17.86	0.00	35.71
RAAx[1]	31.43	17.03	−16.67	56.67	97.66	25.92	29.67	143.00	70.00	30.00	0.00	0.00	0.00	100.00	0.00	0.00	0.00
RAAx[2]	20.67	23.36	−19.33	51.00	91.00	31.96	38.33	134.33	77.78	22.22	0.00	0.00	0.00	100.00	0.00	0.00	0.00
LAAx[1]	30.09	19.75	−35.67	57.00	96.44	26.00	26.67	150.67	70.00	30.00	0.00	0.00	0.00	100.00	0.00	0.00	0.00
LAAx[2]	31.29	15.78	−4.00	48.67	99.75	34.99	50.00	154.33	87.50	12.50	0.00	0.00	0.00	100.00	0.00	0.00	0.00
LAAx[3]	40.33	NC	40.33	40.33	86.33	NC	86.33	86.33	100.00	0.00	0.00	0.00	0.00	100.00	0.00	0.00	0.00
S	−9.43	27.75	−55.67	33.33	82.23	45.28	−12.33	181.67	4.76	14.29	9.52	0.00	71.43	4.55	27.27	0.00	68.18
CrM	30.21	11.92	10.67	52.00	96.08	37.40	33.00	174.67	75.00	25.00	0.00	0.00	0.00	75.00	25.00	0.00	0.00
MTB	20.10	18.93	−26.00	50.67	85.76	26.59	43.33	134.67	62.50	33.33	4.17	0.00	0.00	87.50	12.50	0.00	0.00
RTB	28.95	15.92	12.33	56.67	105.66	13.04	84.33	120.00	66.67	33.33	0.00	0.00	0.00	83.33	16.67	0.00	0.00
LTB	18.53	22.35	−39.67	39.67	90.25	47.31	4.67	178.67	58.33	33.33	8.33	0.00	0.00	91.67	8.33	0.00	0.00

Abbreviations: CDC, caudal deep cervical; CrM, cranial mediastinal; Het, heterogeneous; Hom, homogeneous; HU, Hounsfield Units, Hyper, hyperattenuating; Hypo, hypoattenuating; Iso, isoattenuating; LAAx[1], LAAx[2] and LAAx[3], left accessory axillary; LAx, left axillary; LDSC[1] and LDSC[2], left dorsal superficial cervical; LLMn, left lateral mandibular; LMMn, left medial mandibular; LMR, left medial retropharyngeal; LP, left parotid; LTB, left tracheobronchial; LVSC, left ventral superficial cervical; MTB, medial tracheobronchial; NC, not calculated; Peri, peripheral enhancement; RAAx[1] and RAAx[2], right accessory axillary; RAx, right axillary; RDSC[1] and RDSC[2], right dorsal superficial cervical; RLMn, right lateral mandibular; RMMn, right medial mandibular; RMR, right medial retropharyngeal; RP, right parotid; RTB, right tracheobronchial; RVSC, right ventral superficial cervical; S Het, slightly heterogeneous; S Hypo, slightly hypoattenuating; S, sternal.

TABLE 4 Distribution of the different shapes of the lymph nodes in each technique

	Computed tomography			Ultrasonography			Anatomy		
Lymph node	Elongated, n (%)	Rounded, n (%)	Miscellaneous, n (%)	Elongated, n (%)	Rounded, n (%)	Miscellaneous, n (%)	Elongated, n (%)	Rounded, n (%)	Miscellaneous, n (%)
RP	0 (0.00)	7 (77.80)	2 (22.20)	0 (0.00)	0 (0.00)	0 (0.00)	3 (100.00)	0 (0.00)	0 (0.00)
LP	0 (0.00)	7 (58.30)	5 (41.70)	1 (100.00)	0 (0.00)	0 (0.00)	3 (100.00)	0 (0.00)	0 (0.00)
RMMn	29 (96.70)	1 (3.30)	0 (0.00)	30 (100.00)	0 (0.00)	0 (0.00)	5 (83.30)	0 (0.00)	1 (16.70)
RLMn	29 (96.70)	1 (3.30)	0 (0.00)	29 (96.70)	1 (3.33)	0 (0.00)	6 (100.00)	0 (0.00)	0 (0.00)
LMMn	29 (96.70)	1 (3.30)	0 (0.00)	29 (96.70)	1 (3.30)	0 (0.00)	6 (100.00)	0 (0.00)	0 (0.00)
LLMn	29 (96.70)	1 (3.30)	0 (0.00)	30 (100.00)	0 (0.00)	0 (0.00)	6 (100.00)	0 (0.00)	0 (0.00)
RMR	9 (30.00)	20 (66.70)	1 (3.30)	27 (90.00)	3 (10.00)	0 (0.00)	3 (100.00)	0 (0.00)	0 (0.00)
LMR	10 (33.33)	19 (63.33)	1 (3.30)	27 (90.00)	3 (10.00)	0 (0.00)	4 (80.00)	1 (20.00)	0 (0.00)
RDSC[1]	12 (48.00)	9 (36.00)	4 (16.00)	21 (72.40)	8 (27.60)	0 (0.00)	0 (0.00)	0 (0.00)	0 (0.00)
RDSC[2]	1 (3.30)	5 (16.70)	24 (80.00)	8 (88.90)	1 (11.1)	0 (0.00)	4 (100.0)0	0 (0.00)	0 (0.00)
RVSC	17 (58.60)	10 (34.50)	2 (6.90)	2 (100.00)	0 (0.00)	0 (0.00)	4 (100.00)	0 (0.00)	0 (0.00)
LDSC[1]	9 (37.50)	9 (37.50)	6 (25.00)	20 (80.00)	5 (20.00)	0 (0.00)	0 (0.00)	0 (0.00)	0 (0.00)
LDSC[2]	1 (3.40)	3 (10.30)	25 (86.20)	5 (83.30)	1 (16.70)	0 (0.00)	6 (100.0)0	0 (0.00)	0 (0.00)
LVSC	14 (56.00)	10 (40.00)	1 (4.00)	1 (50.00)	1 (50.00)	0 (0.00)	4 (100.00)	0 (0.00)	0 (0.00)
CDC	6 (54.50)	5 (45.50)	0 (0.00)	0 (0.00)	0 (0.00)	0 (0.00)	0 (0.00)	0 (0.00)	0 (0.00)
RAx	15 (51.70)	14 (48.30)	0 (0.00)	24 (80.00)	6 (20.00)	0 (0.00)	4 (100.00)	0 (0.00)	0 (0.00)
LAx	14 (50.00)	14 (50.00)	0 (0.00)	19 (65.50)	10 (34.50)	0 (0.00)	3 (100.00)	0 (0.00)	0 (0.00)
RAAx[1]	26 (86.70)	4 (13.30)	0 (0.00)	5 (100.00)	0 (0.00)	0 (0.00)	1 (100.00)	0 (0.00)	0 (0.00)
RAAx[2]	3 (33.30)	6 (66.70)	0 (0.00)	1 (100.00)	0 (0.00)	0 (0.00)	0 (0.00)	0 (0.00)	0 (0.00)
LAAx[1]	25 (83.30)	5 (16.70)	0 (0.00)	3 (100.0)0	0 (0.00)	0 (0.00)	1 (100.00)	0 (0.00)	0 (0.00)
LAAx[2]	4 (50.00)	4 (50.00)	0 (0.00)	0 (0.00)	0 (0.00)	0 (0.00)	0 (0.00)	0 (0.00)	0 (0.00)
LAAx[3]	0 (0.00)	1 (100.00)	0 (0.00)	0 (0.00)	0 (0.00)	0 (0.00)	0 (0.00)	0 (0.00)	0 (0.00)
S	15 (68.20)	7 (31.80)	0 (0.00)	7 (41.20)	10 (58.80)	0 (0.00)	3 (75.00)	1 (25.00)	0 (0.00)
CrM	9 (56.30)	7 (43.8)	0 (0.00)	0 (0.00)	0 (0.00)	0 (0.00)	4 (80.00)	1 (20.00)	0 (0.00)
MTB	12 (50.00)	12 (50.00)	0 (0.00)	0 (0.00)	0 (0.00)	0 (0.00)	6 (100.00)	0 (0.00)	0 (0.00)
RTB	0 (0.00)	5 (83.30)	1 (16.70)	0 (0.00)	0 (0.00)	0 (0.00)	5 (83.30)	1 (16.70)	0 (0.00)
LTB	4 (33.30)	7 (58.30)	1 (8.30)	0 (0.00)	0 (0.00)	0 (0.00)	5 (83.30)	1 (16.70)	0 (0.00)

Abbreviations: CDC, caudal deep cervical; CrM, cranial mediastinal; LAAx1, LAAx2, and LAAx3, left accessory axillary; LAx, left axillary; LDSC1 and LDSC2, left dorsal superficial cervical; LLMn, left lateral mandibular; LMMn, left medial mandibular; LMR, left medial retropharyngeal; LP, left parotid; LTB, left tracheobronchial; LVSC, left ventral superficial cervical; MTB, medial tracheobronchial; RAAx1 and RAAx2, right accessory axillary; RAx, right axillary; RDSC1 and RDSC2, right dorsal superficial cervical; RLMn, right lateral mandibular; RMMn, right medial; RMR, right medial retropharyngeal mandibular; RP, right parotid; RTB, right tracheobronchial; RVSC, right ventral superficial cervical; S, sternal.

TABLE 5 Ultrasonographic features of the identified lymph nodes of the head, neck, forelimb, and thorax in healthy cats

	Echogenicity (%)			
Lymph node	Isoechoic	Hypoechoic	Hyperechoic	Heterogeneous
LP	0.00	100.00	0.00	0.00
RMMn	10.00	83.33	0.00	6.67
RLMn	10.00	90.00	0.00	0.00
LMMn	10.00	86.67	0.00	3.33
LLMn	6.67	93.33	0.00	0.00
RMR	23.33	66.67	0.00	10.00
LMR	13.33	73.33	0.00	13.33
RDSC[1]	3.45	82.76	0.00	13.79
RDSC[2]	11.11	88.89	0.00	0.00
RVSC	0.00	50.00	0.00	50.00
LDSC[1]	3.85	76.92	3.85	15.38
LDSC[2]	16.67	66.67	0.00	16.67
LVSC	5000	0.00	0.00	50.00
RAx	46.67	16.67	16.67	20.00
LAx	37.93	17.24	17.24	27.59
RAAx[1]	20.00	60.00	0.00	20.00
RAAx[2]	0.00	100.00	0.00	0.00
LAAx[1]	33.33	66.67	0.00	0.00
S	47.06	35.29	5.88	11.76

Abbreviations: LAAx[1], left accessory axillary; LAx, left axillary; LDSC[1] and LDSC[2], left dorsal superficial cervical; LLMn, left lateral mandibular; LMMn, left medial mandibular; LMR, left medial retropharyngeal; LP, left parotid; LVSC, left ventral superficial cervical; RAAx[1] and RAAx[2], right accessory axillary; RAx, right axillary; RDSC[1] and RDSC[2], right dorsal superficial cervical; RLMn, right lateral mandibular; RMMn, right medial mandibular; RMR, right medial retropharyngeal; RVSC, right ventral superficial cervical; S, sternal.

aspect of the tympanic bullae and *M. longus colli* at the level of the first two cervical vertebrae, and lateral to the carotid sheath. Following these anatomic landmarks, the right and left medial retropharyngeal lymph nodes were identified in all the cats in the imaging study (Figure 4a–d).

3.4 | Superficial cervical lymph center (lymphocentrum cervicale superficiale)

Bilaterally, one dorsal and one ventral superficial cervical lymph nodes were identified in almost all cats of the anatomic study. The dorsal superficial cervical lymph node was located deep to the *M. trapezium* and *M. omotransversarius*, associated with the superficial cervical blood vessels and surrounded by fat. The ventral superficial cervical lymph node was located dorsal and slightly cranial to the junction of the superficial cervical vein with the external jugular vein (Figure 5a). Two dorsal and one ventral superficial cervical lymph nodes on each side were commonly visualized on CT and US images (Figure 5b–d). The dorsal superficial cervical lymph nodes were divided into the most dorsally and the most ventrally located. The most dorsally located lymph node was found deep to the *M. trapezium* and close to the cranial angle of the scapula. The most ventrally located lymph node was found deep to the *M. trapezium* and *M. omotransversarius* slightly cranial to the midcranial border of the scapula. The ventral superficial cervical lymph nodes were identified in the same position described in the anatomic study. The identification of all the superficial cervical lymph nodes on both sides was not possible in all the cats with US.

3.5 | Deep cervical lymph center (lymphocentrum cervicale profundum)

The middle or caudal deep cervical lymph nodes were not visualized in either the anatomic or the US examinations. However, on CT images one caudal deep cervical lymph node was found in 11 cats. This lymph node lied in the fat that is slightly cranial to the thoracic inlet, between the trachea and the *M. sternocephalicus*.

3.6 | Axillary lymph center (lymphocentrum axillare)

In the anatomic study, the axillary lymph nodes were often found bilaterally. The localization was immediately caudal to the axillary vessels at the level of the first intercostal space on each side of the thorax (Figure 6a). On CT images, the axillary lymph nodes were

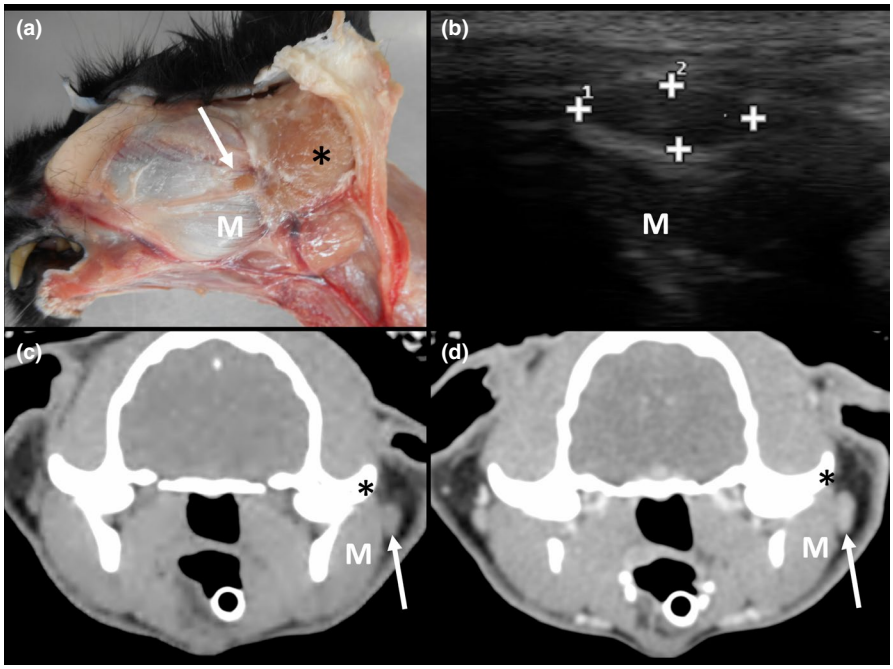

FIGURE 2 Parotid lymph node. (a) Image of the dissection showing the localization of the parotid lymph node (arrow) rostral to the parotid salivary gland (asterisk) and superficial to the *M. masseter* (M). (b) Ultrasonographic image showing an elongated, hypoechoic parotid lymph node between cursors, the *M. masseter* (M), is seen in the far-field. (c, d) Computed tomography (CT) images indicating the localization of an isoattenuating parotid lymph node (arrow) in the precontrast image (c) with homogeneous contrast enhancement pattern (d). The *M. masseter* (M) and the zygomatic arch (asterisk) are indicated

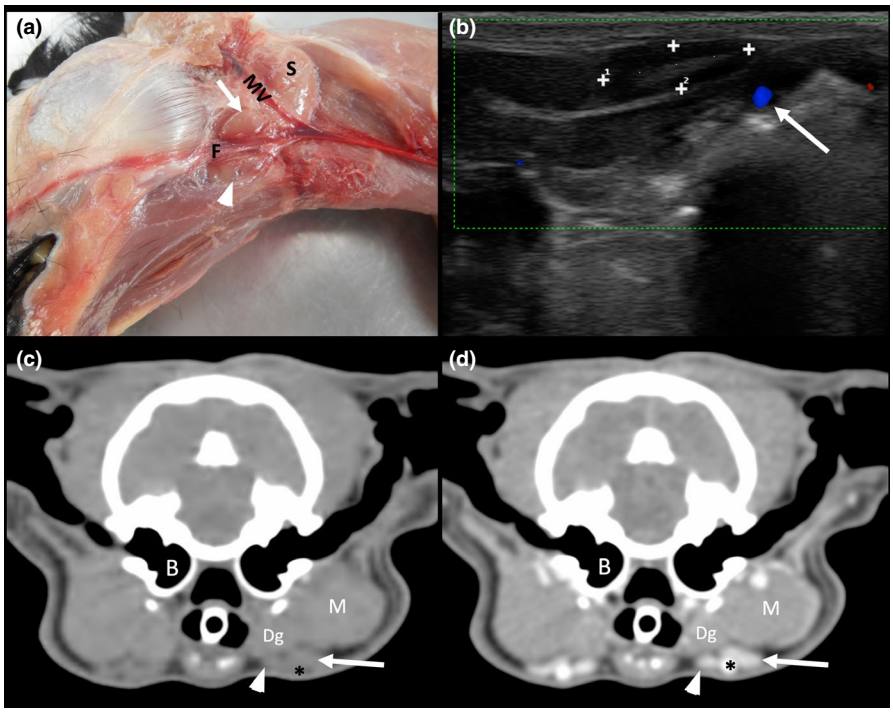

FIGURE 3 Mandibular lymph nodes. (a) Image of the dissection showing the localization of the mandibular lymph nodes (long arrow = lateral; arrowhead = medial) rostral to the mandibular salivary gland (S). The linguofacial (F) and maxillary (MV) veins are indicated. (b) Ultrasonographic image showing a transverse plane of a right lateral mandibular lymph node between cursors. Color Doppler shows the linguofacial vein (blue) medial to the lymph node. (c, d) Computed tomography (CT) images indicating the localization of an isoattenuating mandibular lymph nodes (long arrow = left lateral; arrow head = left medial) in the precontrast image (c) and homogeneous enhancement in the postcontrast image (d). The linguofacial vein is indicated (asterisk). The *M. masseter* (M), *M. digastric* (Dg), and tympanic bulla (B) are indicated

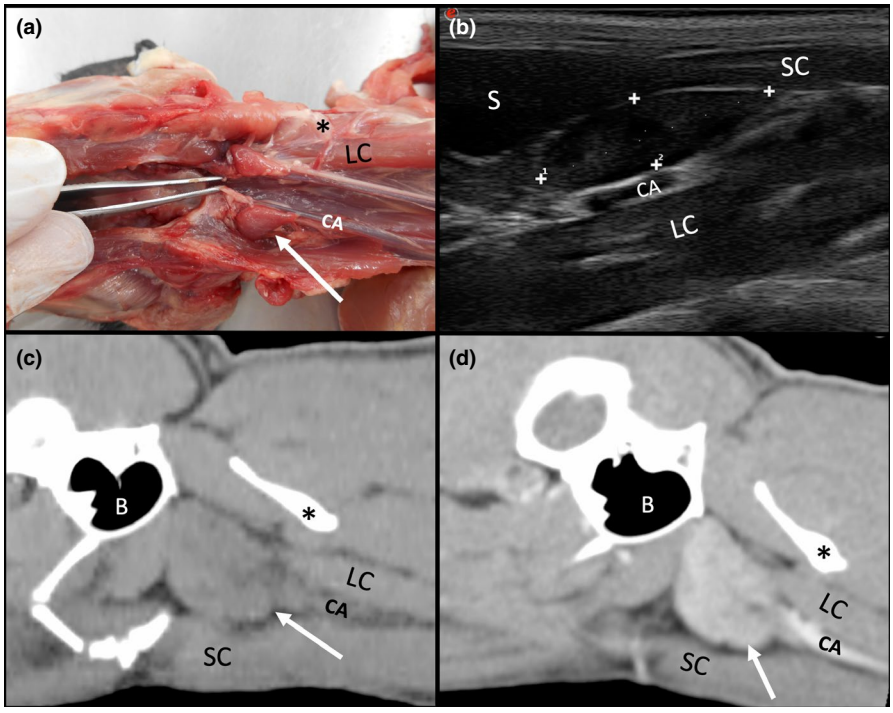

FIGURE 4 Medial retropharyngeal lymph nodes. (a) Image of the dissection showing the localization of the medial retropharyngeal lymph nodes (arrow) ventral to the first cervical vertebra (asterisk). The carotid artery (CA) and the *M. longus colli* (LC) are indicated. (b) Ultrasonographic image showing an elongated and hypoechoic medial retropharyngeal lymph node (between cursors) located caudal to the mandibular salivary gland (S), ventro-medial to the partially seen carotid artery (CA), and the *M. longus colli* (LC). The *M. sternocephalicus* (SC) is indicated. (c, d) Computed tomography (CT) images indicating the localization of the medial retropharyngeal lymph node (arrow); in the precontrast image (c) the elongated isoattenuating node is visible caudo-ventral to the tympanic bulla (B), ventral to the *M. longus colli* (LC) at the level of the first cervical vertebra (asterisk). The postcontrast image (d) shows a slightly heterogeneous contrast enhancement pattern. The *M. sternocephalicus* (SC) is indicated

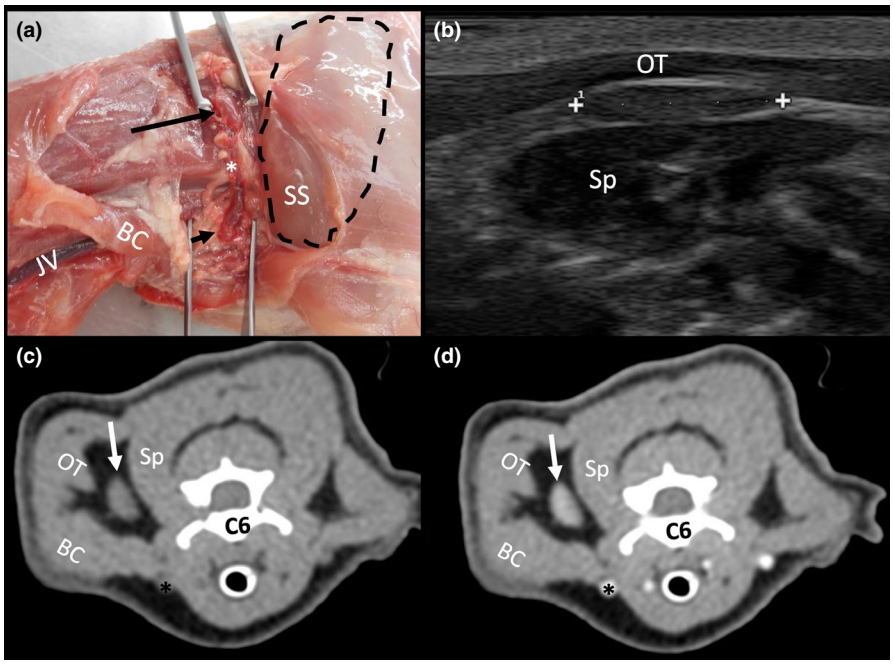

FIGURE 5 Superficial cervical lymph node. (a) Image of the dissection showing the localization of the superficial cervical lymph nodes (long arrow = dorsal; short arrow = ventral), cranial to the scapula (delineated area). The superficial cervical vessels (asterisk) are seen between the two nodes. The *M. brachiocephalic* (BC) and *M. supraspinatus* (SS) and the jugular vein (JV) are indicated. (b) Ultrasonographic image showing an elongated, hypoechoic dorsal superficial cervical lymph node between cursors deep to the *M. omotransversarius* (OT). Medial to the lymph node, the *M. splenius* (Sp) is indicated. (c, d) Computed tomography (CT) images indicating the localization of a slightly hypoattenuating dorsal superficial cervical lymph node (arrow) in the precontrast image (c), with a homogeneous contrast enhancement pattern in the post-contrast image (d). The sixth cervical vertebra (C6), the jugular vein (asterisk), the *M. brachiocephalic* (BC), *M. omotransversarius* (OT), and *M. splenius* (Sp) are indicated

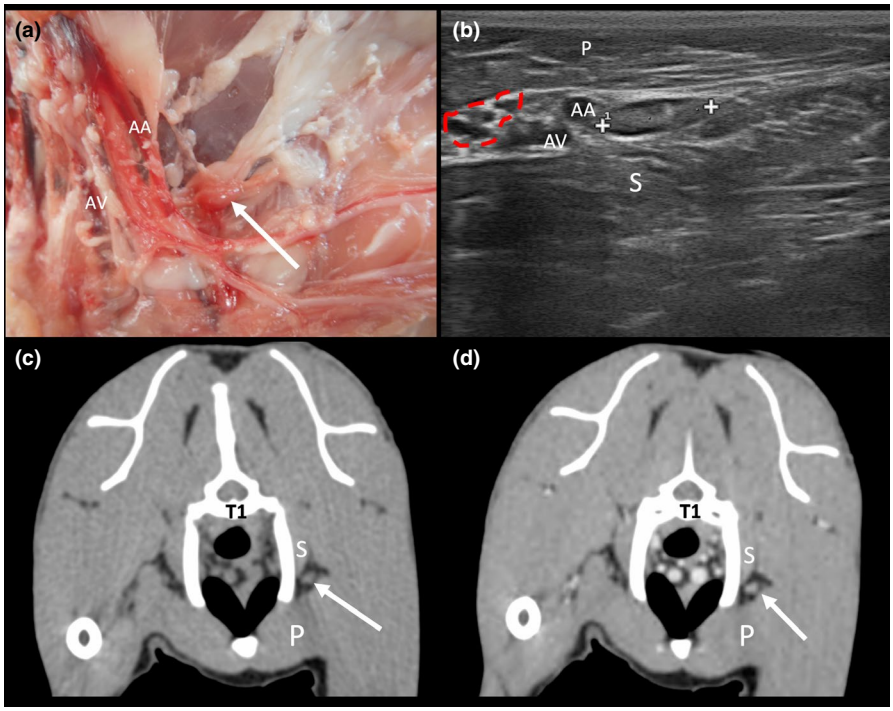

FIGURE 6 Axillary lymph nodes. (a) Image of the dissection showing the localization of the axillary lymph node (arrow) embedded in the fat caudally to the axillary vessels (axillary vein = AV; axillary artery = AA). (b) Ultrasonographic image showing a heterogeneous axillary lymph node (between cursors). A large central hyperechoic center with a hypoechoic periphery is seen. The lymph node is located caudal to the axillary vessels (axillary vein = AV; axillary artery = AA); the *M. pectoralis* (P) is ventral to the lymph node (top part of the image is ventral). Part of the brachial plexus (delineated area) and the *M. scalenus* (S) are indicated. (c, d) Computed tomography (CT) images indicating the localization of a slightly hypoattenuating axillary lymph node (arrow) in the precontrast image (c) with a homogeneous contrast enhancement pattern in the postcontrast image (d). The first thoracic vertebra (T1), the *M. pectoralis* (P), and *M. scalenus* (S) are indicated

identified in almost all the cats bilaterally (Figure 6c,d). The presence of a central hypoattenuating area with negative attenuation values (−29.7 HU) similar to fat attenuation was identified. This hypoattenuating tissue within the lymph node was surrounded by a peripheral ring-shaped tissue that corresponded to the normal attenuation of lymphatic tissue. The ROIs for the measurement of the Hounsfield units were placed, as possible, in this peripheral tissue. However, the inclusion of part of the center in smaller lymph nodes was sometimes challenging to avoid, resulting in a negative HU in the average attenuation for these lymph nodes. On US, the echogenicity of the axillary lymph nodes was the most variable among lymph nodes (Table 5). Some lymph nodes presented a large hyperechoic center with a more hypoechoic periphery (Figure 6b).

Another component of this lymph center is the accessory axillary lymph node. It was found bilaterally in 1/6 cats in the anatomic study, along the lateral thoracic vessels. On CT, one to three accessory axillary lymph nodes were bilaterally identified. A single lymph node located at the level of the third costochondral joint, adjacent to the dorsal border of the *M. pectoralis profundus*, was most commonly seen on both sides (Figure 7a–d). Additionally, one or two lymph nodes were identified more caudally. The most caudal lymph node was almost reaching the costal arch and in contact with the dorsal border of the *M. pectoralis profundus*. The frequency of visualization of these lymph nodes using US was low (Table 1).

3.7 | Dorsal thoracic lymph center (lymphocentrum thoracicum dorsale)

The aortic thoracic and the intercostal lymph nodes are described as components of this lymph center. However, they were not visible in this study.

3.8 | Ventral thoracic lymph center (lymphocentrum thoracicum ventrale)

The only member of this lymph center that was identified was the sternal lymph node. The superficial cranial epigastric lymph node (former xiphoid lymph node) and the phrenic lymph node were not visible in the anatomy or the imaging study. A single sternal lymph node was identified at the dorsal aspect of the third sternebra, in contact with the internal thoracic vessels. On CT transverse images, a single sternal lymph node presented a hypoattenuating center surrounded by a peripheral ring-shaped lymphoid tissue, as described for the axillary lymph nodes. Because of this, a negative HU in the average attenuation for this lymph node was also obtained. On US images, the visualization of the sternal lymph nodes was challenging due to the artifacts caused by the lungs. However, 17 identified lymph nodes presented a hyperechoic central line consistent with the hilus (Figure 8a–d).

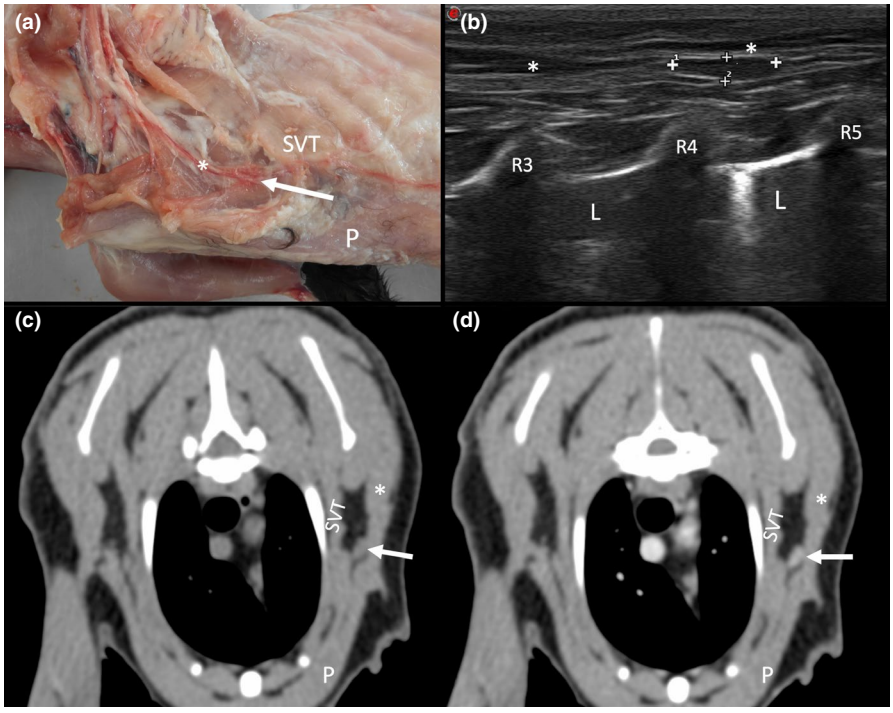

FIGURE 7 Accessory axillary lymph node. (a) Image of the dissection showing the localization of the accessory axillary lymph node (arrow) around the fourth intercostal space, along the lateral thoracic vessels (asterisk), between the *M. pectoralis* (P) and *M. serratus ventralis thoracicus* (SVT). (b) Ultrasonographic image showing an elongated, hypoechoic left accessory axillary lymph node between cursors, deep to the cutaneous muscles (asterisks). The third, fourth, and fifth ribs (R3, R4, and R5) and the lung field (L) are indicated. (c, d) Computed tomography (CT) images indicating the localization of a slightly hypoattenuating accessory axillary lymph node (arrow) in precontrast (c) with a homogeneous contrast enhancement pattern in the postcontrast image (d), dorsal to the *M. pectoralis* (P) and between the *M. serratus ventralis thoracicus* (SVT) and the *M. latissimus dorsi* (asterisk)

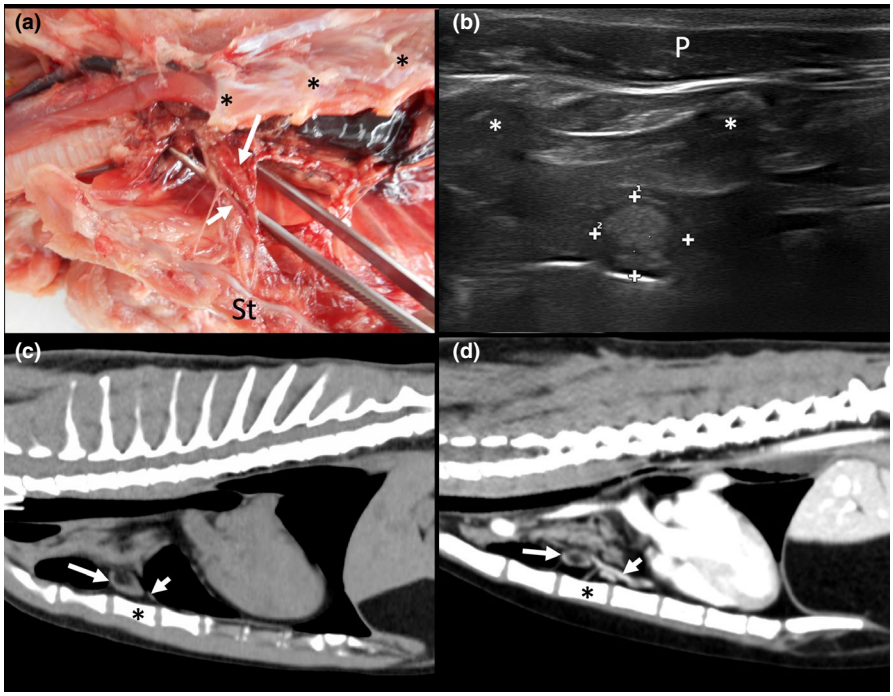

FIGURE 8 Sternal lymph node. (a) Image of the dissection after parasternal thoracotomy showing the localization of the sternal lymph node (long arrow) along the internal thoracic vessels (short arrow) at the cranio-ventral aspect of the thorax. The sternum (St) has been ventrally pulled to allow the visualization of the lymph node. (b) Ultrasonographic image showing a rounded lymph node with a hyperechoic center and hypoechoic periphery between cursors. The second and third ribs (asterisks) and the *M. pectoralis* (P) are indicated. (c, d) Computed tomography (CT) sagittal images indicating the localization of the sternal lymph node in precontrast (c) and postcontrast (d) images (long arrows). The hypoattenuating center compatible with a fatty hilus is visible. The third sternebra (asterisk) and internal thoracic vessels (short arrow) are indicated

3.9 | Mediastinal lymph center (lymphocentrum mediastinale)

One cranial mediastinal lymph node was identified in the anatomic study between the trachea and the major blood vessels. In CT images, 1 cranial mediastinal lymph node was identified in 15 cats, and 2 were seen in 1 cat. Assessment of this lymph center using US in healthy cats was not achievable due to the impossibility to find an acoustic window to avoid the normal pulmonary tissue.

3.10 | Bronchial lymph center (lymphocentrum bronchale)

In the anatomic study, three tracheobronchial lymph nodes were found corresponding to the right, left, and middle tracheobronchial lymph nodes. The right tracheobronchial lymph node was visible between the main right bronchus and the azygos vein. The left tracheobronchial lymph node was visible between the main left bronchus and the left pulmonary artery. The middle tracheobronchial lymph node was found caudally to the carina tracheae (Figure 9a). On CT, the use of postcontrast images and multiplanar reconstructions for the localization of these lymph nodes was fundamental. On sagittal reconstruction, the middle tracheobronchial lymph node was identified between the carina and the pulmonary blood vessels, improving its identification in other planes. Similarly, the right and left tracheobronchial lymph nodes were localized (Figure 9b–d). On US, it was impossible to obtain an acoustic window that allowed the assessment of this lymph center.

4 | DISCUSSION

To the authors' knowledge, this is the first report of the normal characteristics of lymph nodes from the head, neck, thorax, and forelimb using CT and US and comparing with an anatomic study in presumably healthy cats. In the anatomic study, lymph node identification was challenging for some lymph centers (e.g., superficial cervical, deep cervical, and dorsal thoracic lymph centers) due to their small size and the amount of fat in which lymph nodes were frequently embedded.

This is the first study reporting the precontrast and postcontrast CT characteristics and dimensions of the mandibular, superficial cervical, deep cervical, axillary, accessory axillary, cranial mediastinal, tracheobronchial and sternal lymph nodes, and the postcontrast CT features of the medial retropharyngeal lymph nodes in healthy cats. In our study, CT generally showed a higher frequency of lymph node identification in comparison to US and anatomy, especially on postcontrast images. This advantage

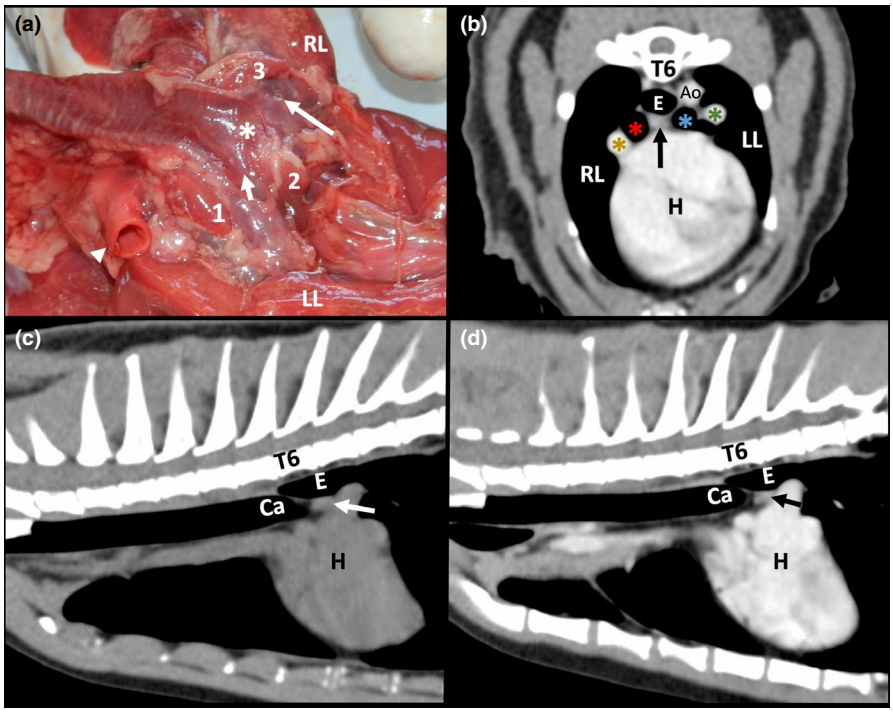

FIGURE 9 Tracheobronchial lymph nodes. (a) Image of the dissection showing the localization of the left (1), middle (2), and right (3) tracheobronchial lymph nodes in relation to the carina (asterisk) and the main bronchi (short arrow = left; long arrow = right). The aorta (arrowhead) and the left (LL) and right (RL) lungs are indicated. (b–d) Computed tomography (CT) images (b, transverse; c, d, sagittal) indicating the localization of an isoattenuating middle tracheobronchial lymph node (arrow) in the precontrast image (c) with a homogeneous contrast enhancement pattern in the postcontrast images (b and d), caudal to the carina (Ca) and ventral to the esophagus (E, with moderate amount of gas in the lumen). The heart (H) and sixth thoracic vertebra (T6) are indicated. In (b) the main bronchi (red asterisk = right; blue asterisk = left), the main pulmonary arteries (yellow asterisk = right; green asterisk = left), the aorta (Ao), and the right (RL) and left LL) lungs are indicated

is likely to be due to the good blood supply of lymph nodes, as well as the cross-sectional aspect, and therefore superior overview of this imaging modality. Well-vascularized organs show an optimal enhancement after the administration of contrast medium which makes them easier to depict, as previously reported (Dennler, 2013). However, when the lymph nodes were closer to blood vessels or another well-vascularized structure (e.g., salivary gland), their differentiation was challenging (e.g., parotid, lateral retropharyngeal, and phrenic and dorsal thoracic lymph nodes) as described in dogs (Kneissl & Probst, 2007). In this study, the body condition of the cats also played an important role in the visualization of the lymph nodes on CT images. When lymph nodes were surrounded by a fair amount of fat, their visualization improved as previously mentioned in dogs (Beukers et al., 2013; Rossi et al., 2011). Another benefit of helical-CT in the assessment of lymph nodes is the possibility to obtain multiplanar reconstructions. This helped in the identification of lymph nodes (e.g., tracheobronchial) and their true anatomical position (e.g., medial retropharyngeal and superficial cervical and tracheobronchial lymph nodes), as well as provided the opportunity to perform more accurate measurements as previously described (Nemanic & Nelson, 2012). In this study, the attenuation of the lymph nodes was similar to previous reports (Beukers et al., 2013; Nemanic & Nelson, 2012; Nyman, 2005). However, the axillary and sternal lymph nodes presented a high percentage of heterogeneous attenuation with a central area of fat attenuation. A fatty hilus has been previously reported for the axillary lymph node, and in our study, a similar situation is presented in the sternal lymph nodes (Sugimura et al., 1956). This could also explain the isoechoic to hyperechoic appearance in US that made their visualization challenging (Nyman & O'Brien, 2007).

This is the first report of the echographic characteristics of the mandibular, superficial cervical, axillary, accessory axillary, and sternal lymph nodes in healthy cats. Ultrasonographic identification of lymph nodes was challenging for some lymph centers. The low image resolution in various areas (e.g., parotid and deep cervical lymph centers) and the impossibility to obtain an acoustic window in the thorax were factors that reduced the identification of some lymph centers (e.g., dorsal thoracic, mediastinal, and bronchial lymph centers). Esophageal endoscopic ultrasonography has been reported as a suitable procedure to assess the tracheobronchial lymph nodes in dogs (Gaschen et al., 2003; St-Vincent & Pharr, 1998). Unfortunately, endoscopic probes were not available in this study. We found that the body condition also affected the visualization of lymph nodes. In various cases, a large amount of fat around the lymph nodes reduced their differentiation during the US evaluation; similar limitations have been reported for dogs in the identification of the axillary lymph node (Nyman, 2005).

In the present study, the measured length, width, and height of the identified lymph nodes were frequently significantly smaller in anatomy when compared to CT and US. We hypothesize that, although the cadavers were fresh and dissection was performed within 24 h after death, the amount of blood and lymph in the lymph nodes varied and may be responsible for the small size in the anatomic study. In the current anatomy literature (Saar & Getty, 1982; Tompkins, 1993), the reported length or diameter of the feline lymph nodes is based on a series of research that included cats from 1 month old to 6 years old (Sugimura et al., 1955, 1956, 1959). It has been reported that age influences the size of lymph nodes; therefore, young animals present larger lymph nodes (Burns, 2008). This could explain the smaller length of the lymph node in our study when compared to the available length in the current literature. Considering this, a previous CT study reported measurements of sternal lymph node in six young cats (8–12 months old) that were similar to our results (Dennler, 2013). Factors that could explain this similarity are unclear. We hypothesized that the relative adult weight of the cat in that study (ranged 2.4–3.6 kg; Dennler, 2013) might be a reason that could explain the similar results with our study. More recently, a study reported similar attenuation values but shorter length for the sternal, cranial mediastinal, and tracheobronchial lymph nodes when compared to this study (Smith et al., 2019). The differences in length can be due to the thicker slices used in the study of Smith which is likely to leave part of the lymph node not included in the reconstructions. Dimensions of the medial retropharyngeal lymph node in cats using CT have been previously described and are similar to our results (Nemanic & Nelson, 2012; Oliveira, 2012).

The medial retropharyngeal, dorsal superficial cervical, and sternal lymph nodes on CT showed the highest differences in length, width, and height when compared with US and anatomy. It has been reported that the oblique natural position of lymph nodes in the body and the position of the forelimbs while scanning influence the true transverse image of the lymph nodes on CT images (Nemanic & Nelson, 2012). This effect might explain the differences found in the measurements of these lymph nodes in our study.

The shapes of the lymph nodes presented in this study are similar to previous reports (Agthe et al., 2009; Beukers et al., 2013; Kneissl & Probst, 2007; Nemanic & Nelson, 2012; Nyman, 2005; Nyman & O'Brien, 2007; Rossi et al., 2011; Sugimura et al., 1955, 1956, 1959). Rounded lymph nodes have been reported as malignant (Llabres-Diaz, 2004; Nyman, 2005; Nyman & O'Brien, 2007). However, in our study, rounded lymph nodes were identified in all the lymph centers and, due to their small size and homogeneous parenchyma in both imaging techniques, were considered as a shape variant rather than a sign of malignancy.

There are several limitations in this study. First, low sample size in the anatomic study due to the low number of deceased cats that matched the inclusion criteria. Second, the variability in the identification of lymph nodes per lymph center resulted in an unequal number of lymph nodes in each cat and for both imaging techniques. Third, all the healthy cats included in the imaging study were carefully evaluated to avoid the inclusion of cats with lymphadenopathy. However, histopathology was not performed to prevent complications and for ethical reasons due to the premise of normal health status of the cats. Fourth, the assessment of lymph nodes was made only one time by the first author (M.T.R); therefore, the interobserver or intraobserver analysis could not be performed.

In conclusion, the identification of lymph nodes in the head, neck, thorax, and forelimb using US and CT is possible. Cats with high body condition showed good contrast on CT for lymph node identification. In thin cats, the administration of contrast medium improved the differentiation of lymph nodes from the surrounding muscles. The axillary and sternal lymph nodes present a relatively large and fatty hilus that creates a different appearance on CT and US images compared to other lymph nodes. Multiplanar reconstruction on CT is a useful tool that increased the accuracy of the size measurements of lymph nodes that have a relative natural oblique location on transverse images (e.g., medial retropharyngeal and superficial cervical lymph nodes). To the authors' knowledge, this is the first report of the lymph nodes dimensions for the head, neck, thorax, and forelimb lymph centers using CT and US and comparing with an anatomic study in presumably healthy cats. The data reported in this study are proposed as reference values.

ACKNOWLEDGMENTS

The authors acknowledge Dr. Oriol Camps for its support in the statistical analysis of the present study. The first author of this study (M.T.R) received financial support by a PhD scholarship from the Colombian Government and Departamento Administrativo de Ciencia, Tecnología e Innovación (COLCIENCIAS). Scholarship program: Becas Francisco José de Caldas, 2010.

CONFLICTS OF INTEREST

The authors declare that there is no conflict of interest.

AUTHOR CONTRIBUTIONS

Conception and Design: Mauricio Tobón Restrepo, Yvonne Espada, Rosa Novellas. Acquisition of Data: Mauricio Tobón Restrepo, Yvonne Espada, Adrià Aguilar, Xavier Moll, Rosa Novellas. Analysis and Interpretation of Data: Mauricio Tobón Restrepo. Drafting the Article: Mauricio Tobón Restrepo. Revising Article for Intellectual Content: Yvonne Espada, Adrià Aguilar, Xavier Moll, Rosa Novellas. Final Approval of the Completed Article: Mauricio Tobón Restrepo, Yvonne Espada, Adrià Aguilar, Xavier Moll, Rosa Novellas.

ORCID

Mauricio Tobón Restrepo https://orcid.org/0000-0001-5487-1408

REFERENCES

Agthe, P., Caine, A.R., Posch, B. & Herrtage, M.E. (2009) Ultrasonographic appearance of jejunal lymph nodes in dogs without clinical signs of gastrointestinal disease. *Veterinary Radiology & Ultrasound*, 50(2), 195–200. https://doi.org/10.1111/j.1740-8261.2009.01516.x.

Beukers, M., Vilaplana Grosso, F. & Voorhout, G. (2013) Computed tomographic characteristics of presumed normal canine abdominal lymph nodes. *Veterinary Radiology & Ultrasound*, 54(6), 610–617. https://doi.org/10.1111/vru.12075

Burns, G.O., Scrivani, P.V., Thompson, M.S. & Erb, H.N. (2008) Relation between age, body weight, and medial retropharyngeal lymph node size in apparently healthy dogs. *Veterinary Radiology & Ultrasound Ultrasound*, 49(3), 277–281. https://doi.org/10.1111/j.1740-8261.2008.00366.x

Dennler, M., Bass, D.A., Gutierrez-Crespo, B., Schnyder, M., Guscetti, F., Di Cesare, A. et al. (2013) Thoracic computed tomography, angiographic computed tomography, and pathology findings in six cats experimentally infected with aelurostrongylus abstrusus. *Veterinary Radiology and Ultrasound*, 54(5), 459–469. https://doi.org/10.1111/vru.12044

Gaschen, L., Kircher, P. & Lang, J. (2003) Endoscopic ultrasound instrumentation, applications in humans, and potential veterinary applications. *Veterinary Radiology and Ultrasound*, 44(6), 665–680. https://doi.org/10.1111/j.1740-8261.2003.tb00530.x

Kneissl, S. & Probst, A. (2007) Comparison of computed tomographic images of normal cranial and upper cervical lymph nodes with corresponding E12 plastinated-embedded sections in the dog. *Veterinary Journal*, 174(2), 435–438. https://doi.org/10.1016/j.tvjl.2006.09.005

Llabres-Diaz, F.J. (2004) Ultrasonography of the medial iliac lymph nodes in the dog. *Veterinary Radiology & Ultrasound*, 45(2), 156–165. https://doi.org/10.1111/j.1740-8261.2004.04026.x

NAV. (2017) *Nomina anatomica veterinaria*, 6th edition. Edited by veterinary gross anatomical nomenclature International committee. Oslo: ICVGAN. Retrieved from http://www.wava-amav.org/downloads/NHV_2017.pdf

Nemanic, S., Hollars, K., Nelson, N.C. & Bobe, G. (2015) Combination of computed tomographic imaging characteristics of medial retropharyngeal lymph nodes and nasal passages aids discrimination between rhinitis and neoplasia in cats. *Veterinary Radiology and Ultrasound*, 56(6), 617–627. https://doi.org/10.1111/vru.12279

Nemanic, S. & Nelson, N.C. (2012) Ultrasonography and noncontrast computed tomography of medial retropharyngeal lymph nodes in healthy cats. *American Journal of Veterinary Research*, 73(9), 1377–1385.

Nyman, H.T., Kristensen, A.T., Skovgaard, I.M. & McEvoy, F.J. (2005) Characterization of normal and abnormal canine superficial lymph nodes using gray-scale B-mode, color flow mapping, power, and spectral doppler ultrasonography: A multivariate study. *Veterinary Radiology and Ultrasound*, 46(5), 404–410. https://doi.org/10.1111/j.1740-8261.2005.00074.x

Nyman, H.T. & O'Brien, R.T. (2007) The sonographic evaluation of lymph nodes. *Clinical Techniques in Small Animal Practice*, 22(3), 128–137. https://doi.org/10.1053/j.ctsap.2007.05.007

Oliveira, C.R., O'Brien, R.T., Matheson, J.S. & Carrera, I. (2012) Computed tomographic features of feline nasopharyngeal polyps. *Veterinary Radiology & Ultrasound*, 53(4), 406–411. https://doi.org/10.1111/j.1740-8261.2012.01931.x

Rossi, F., Patsikas, M.N. & Wisner, E.R. (2011) Abdominal lymph nodes and lymphatic collecting system. In: Schwarz, T. and Saunders, J.H. (Eds.) *Veterinary computed tomography*. Ames, IA: Wiley-Blackwell, pp. 371–379.

Saar, L.I. & Getty, R. (1982) Sistema linfático de los carnívoros. In: Getty, R. (Ed.) *S.Sisson - J.D.Grossman. Anatomía de los animales domésticos*, 5th edition. Barcelona, Spain: Masson, pp. 1811–1831.

Smith, A.J., Sutton, D.R. & Major, A.C. (2019) CT appearance of presumptively normal intrathoracic lymph nodes in cats. *Journal of Feline Medicine and Surgery*, 22(10), 875–881. https://doi.org/10.1177/1098612X19886672

St-Vincent, R.S. & Pharr, J.W. (1998) Transesophageal ultrasonography of the normal canine mediastinum. *Veterinary Radiology & Ultrasound*, 39(3), 197–205.

Sugimura, M., Kudo, N. & Takahata, K. (1955) Studies on the lymphonodi of cats: I. Macroscopical observations on the lymphonodi of heads and necks. *Japanese Journal of Veterinary Research*, 3(2), 90–104.

Sugimura, M., Kudo, N. & Takahata, K. (1956) Studies of lymphonodi of cats: II. Macroscopical observations on the lymphonodi of the body surfaces, thoracic and pelvic limbs. *Japanese Journal of Veterinary Research*, 4(3), 101–112.

Sugimura, M., Kudo, N. & Takahata, K. (1959) Studies on the lymphonodi of cats: IV. Macroscopical observations on the lymphonodi in the thoracic cavity and supplemental observations on those in the head and neck. *Japanese Journal of Veterinary Research*, 7(1–4), 27–51.

Tompkins, M.B. (1993) Lymphoid system. In: Hudson, L.C. and Hamilton, W.P. (Eds.) *Atlas of feline anatomy for veterinarians*, 1st edition. Philadelphia, PA: W.B. Saunders Company, pp. 113–126.

How to cite this article: Tobón Restrepo M, Espada Y, Aguilar A, Moll X, Novellas R. Anatomic, computed tomographic, and ultrasonographic assessment of the lymph nodes in presumed healthy adult cats: The head, neck, thorax, and forelimb. *J Anat*. 2021;00:1–18. https://doi.org/10.1111/joa.13429